archives
of thermodynamics
Vol. **40**(2019), No. 1, 145–160
DOI: 10.24425/ather.2019.128295

Modeling of the impact of construction solutions on operating parameters of the internal heat exchanger with refrigerant R744

JAKUB JANUS[*a]
PRZEMYSŁAW JAN SKOTNICZNY[a]
MARIA RICHERT[b]

[a] Strata Mechanics Research Institute of Polish Academy of Science, Reymonta 27, 30-059 Kraków, Poland

[b] AGH University of Science and Technology, Faculty of Non-Ferrous Metals, Mickiewicza 30, 30-059 Krakow, Poland

Abstract Work on increasing the efficiency of heat exchangers used in car air conditioning systems may lead to a partial change in the construction of refrigeration systems. One of such changes is the use of smaller gas coolers, which directly translates into a reduction in the production costs of the entire system. The article presents the use of computational fluid dynamics methods to simulate the impact of changing the shape of an internal heat exchanger on the cooling efficiency with R744 as the refrigerant. Internal heat exchangers with different geometry of the outer channels were subjected to numerical analysis. The obtained results of calculations show temperature changes in inner and outer channels on the length of the heat exchanger.

Keywords: Heat exchanger; Internal heat exchanger; Cooling efficiency; Numerical fluid mechanics

[*]Corresponding Author. Email: janus@img-pan.krakow.pl

1 Introduction

Internal heat exchanger (IHX) is a liquid-to-vapor heat exchanger, with one inner chamber and one outer chamber. Hot liquid refrigerant from the condenser flows through the inside chamber, and it's surrounded by cool refrigerant vapor flowing from the evaporator through the outer chamber. The task of the heat exchanger is to increase the efficiency of the system by subcooling the liquid refrigerant, which is supplied to the evaporator by refrigeration control devices.

Over time, it was necessary to miniaturize refrigeration systems, which entails the need to increase the efficiency of heat exchangers. This action forces scientists to conduct research and developments on various methods that increase the efficiency of internal heat recovery. Among the ways of improving the systems efficiency, there are various techniques to improve heat transport, just to mentionchanges in refrigerant as well as changes of exchanger geometry. In papers [1,2,3] due to the changes of the upper layer geometry of the plate heat exchanger as well as in [4] due to the general change of internal heat exchanger geometry, improvement in heat transport efficiency was achieved. These works allow the develop more energy-efficient and efficient heating ventilation and air (HVAS) systems.

Heat exchangers used in automotive industry are subject to a prescribed regulation regarding the refrigerants used in the system. In order to assess the harmful effect impact of the refrigerant on the atmosphere, the GWP (global warming potential) coefficient was introduced. On January 1, 2011, according to the EU Directive 2006/40/EU, in all newly produced refrigeration and air conditioning equipment, the fluids not exceeding GWP coefficient above level 150 must be applied. According to the directive, it was proposed that the refrigerant R134a (ratio GWP = 1430) should be replaced with R744 (CO_2) featuring the GWP = 1. For these reasons, the proposal of changing the refrigerant is not ecologically and economically justified. It is necessary to focus on the shape of exchanger and appropriate materials selection from which it is built using a refrigerant in the form of CO_2.

In 1998, the works on the use of CO_2 refrigerant in the automotive industry were initiated [5], but from year 2005 it was proposed to replace the refrigerant R134a by R744 [6,7]. At the same time, research into the use of CO_2 for internal heat exchangers in refrigeration and air-conditioning systems began [8,9]. A few years later, experimental analyzes of internal heat exchanger refrigeration systems optimization were presented [10,11].

The scheme of the car air-conditioning system is shown in Fig. 1. The air conditioning system primarily consists of a compressor, evaporator and a condenser. The cooling medium circulating in a closed circuit is pumped to the compressor. Than it is transported to the condenser where the working fluid is converted into a liquid form. Thanks to the fans, the desired process temperature is maintained. Then, the liquid gas is transported throughout internal heat exchanger to the evaporator where the temperature drops dramatically in the expansion process. The purpose of the internal heat exchanger is to subcool the liquid in the tube B through a cooler gas in the tube A, which increases the efficiency of the air-conditioning system.

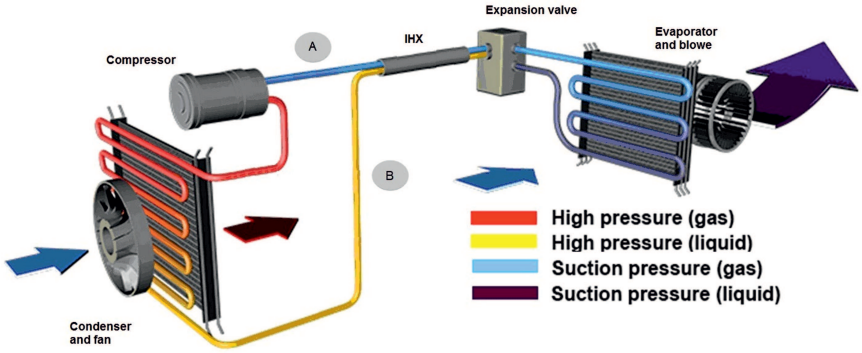

Figure 1: Scheme of the car air-conditioning system [12].

There is also research to develop new construction of heat exchangers. One of such constructions is a heat exchanger with microjets [13] or mini- and microchannels technology [14,15]. Thanks to such solution it is possible to obtain higher values of the heat transfer coefficient in the exchanger.

The use of computer techniques in the form of numerical simulations using the finite volume method known as CFD (computational fluid dynamics) offers great opportunities for developments in this area. This technique gives the opportunity to visualize various phenomena, such as fluid flows, temperature distribution, or stress distribution. Huge advantage of CFD is the ability to simulate these phenomena in both 2D and 3D space. An extensive literature review in the field of designing various types of heat exchangers using CFD methods is presented in [16]. The authors, in their analysis of 66 literature items, found the high usefulness of computer simulation methods, providing the possibility of quick and economical solving

of the design problems of heat exchangers. Authors shown the flexibility of these methods, which can be used in the initial design stage by forecasting the fluid flow, and at the final stage in the form of optimizing the shape of the exchanger itself. One of the works using CFD methods in research on heat exchangers is the publication [17], in which the authors focus on the optimization of the internal heat exchanger for refrigeration, where the refrigerant is CO_2. Experimental and numerical research on microchannels of radiators used in car air-conditioning systems is also being carried out in work [18].

The purpose of the work was to perform simulation calculations of the impact of geometry changes in the heat exchanger on the cooling efficiency of R744 refrigerant (CO_2). It was decided to perform an analysis for three types of geometries, differing in the way of conducting the outer channels in the exchanger.

2 Numerical simulation

2.1 Calculation area

Numerical calculations were carried out for three models of the tube in tube counter current heat exchanger with a length of 1.0 m . In model I, the geometry was presented as a typical 'pipe in pipe' exchanger. Model II corresponded to the geometry in which 16 outer channels (heated) were made parallel to the inner channel (heating). In model III, geometry of outer channels have been twisted around inner channel (Fig. 2).

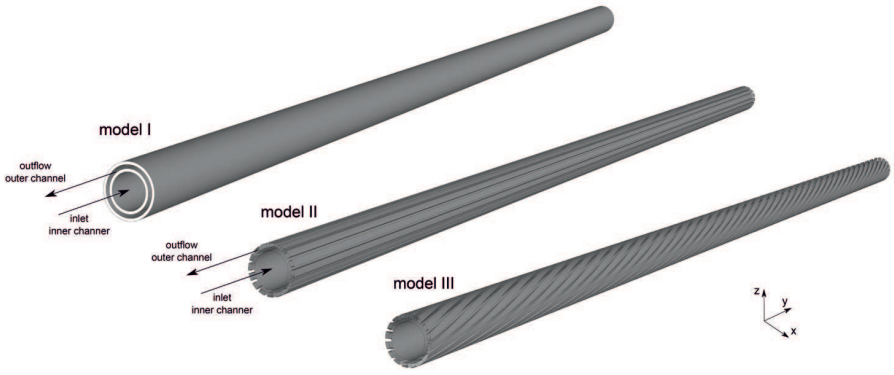

Figure 2: Internal heat exchanger models.

All three models consisted of an inner channel with radius of 16.4 mm. In model I, the inside radius of the outer channel was 9.5 mm, while the external radius is equal to 11.2 mm (Fig. 3). For model II and model III, the outer channel consist of 16 channels with cross-section and dimensions shown in Fig. 4. The outer radius of exchanger was 12.5 mm. Total length of three exchanger models was 1.0 m.

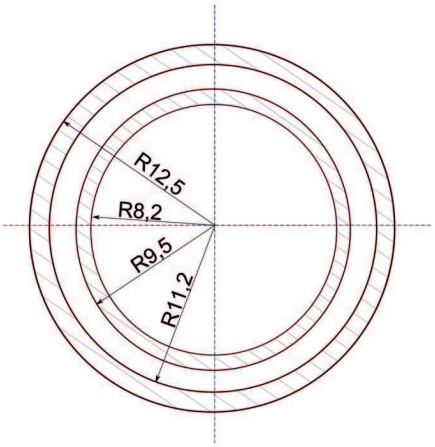

Figure 3: Heat exchanger cross-section – model I.

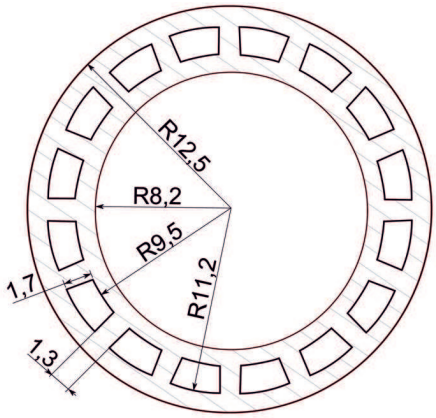

Figure 4: Heat exchanger cross-section – model II.

The outer channels in the II model had shape of a simple prism, while in the III model outer channels were wound along the exchanger in accordance with the parametric curve equation, which was surface extraction trajectory performed as a script in the preprocessing program:

$$s = 2\pi r \cot\_10\,, \tag{1}$$

$$\theta = \frac{L}{s}\, t\, 360\,, \tag{2}$$

$$z = t\, L\,, \tag{3}$$

where: $\cot\_10$ – cotangent of the helix angle on the pitch diameter 10 mm, s – distance of the forming cylinder between the nearest points of helix, r – cyllinder radius, L – curve total lenght, θ – rotation angle of the pull-out surface, z – position in the axis, t – parameter of moving along the trajectory from 0 to 1.

In order to obtain correct numerical calculation results, it was necessary to apply a dense calculation mesh. It was decided to use the mesh size

function, which allows to control the size of numerical mesh around the selected point, edge or surface [1]. Three-dimensional model of the internal heat exchanger was digitized with the unstructured tetrahedral mesh (Fig. 5), which then, due to the large size of the model and selection of a dense computing mesh, was converted into a polyhedral mesh (Fig. 6). The advantage of using this type of mesh is to obtain more accurate results by converting bad cells and faster obtaining the final results due to the smaller number of cells compared to the tetrahedral mesh. Mesh conversion was made by using the Ansys Fluent 18 software. The mesh consist of 2.15 million elements for all three geometrical models.

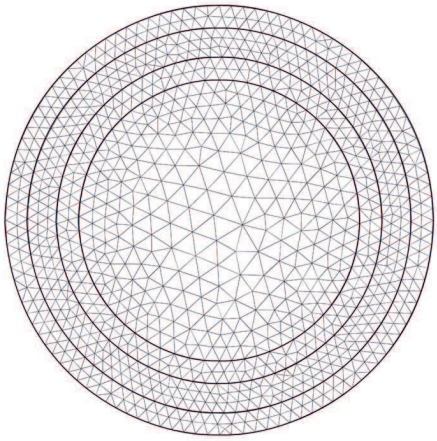

Figure 5: Polyhedral mesh of model I.

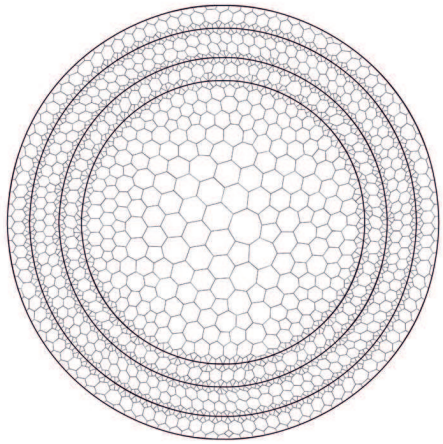

Figure 6: Tetrahedral mesh of model I.

2.2 Boundary conditions and flow model

In the studied issue, there are two centers, gas (also in the supercritical state) in the form of CO_2 and a solid in the form of an aluminum alloy.

The boundary condition for the inner channel HP (heating) and outer channels LP (heated) has been defined as a mass flow. The design assumptions set static pressure at the inlet to the channels equal to:

$$P_{HP} = 12.00\,,$$

$$P_{LP} = 4.50\,,$$

where: P_{HP} – inlet pressure for inner channel (heating), P_{LP} – inlet pressure for outer channels (heated).

Due to the flow nature, it was necessary to define the outlet form individual channels as a pressure outlet, which entails defining the pressure at the outlet of the channels. Therefore, it was necessary to estimate the CO_2 pressure drop due to flow resistance. For this purpose, the Darcy-Waisbach equation was used:

$$\Delta p = \lambda \frac{L}{D_h} \frac{\rho u^2}{2}, \tag{4}$$

where: Δp – denote the pressure loss, λ – flow coefficient, dependent on the Reynolds number, L –length of the channel, D_h – hydraulic diameter, ρ – fluid density, u – fluid velocity.

Fluid velocity is determined by the formula

$$u = \frac{Q_m}{\rho S}, \tag{5}$$

where: Q_m – mass flow rate, S – cross-section area.

The Reynolds number is defined by the formula

$$\mathrm{Re} = \frac{u D_h}{\nu}, \tag{6}$$

where: u – fluid velocity, Dh – hydraulic diameter, ν – fluid kinematic viscosity.

Assuming the cross-section area and mass flow rate in Eq. (5), fluid velocities were calculated. By defining the characteristic dimension in the Eq. (6) as a hydraulic diameter, and assuming the CO_2 kinetic viscosity at 13 °C and 60 °C, the Reynolds numbers were calculated (Tab. 1).
In engineering practice, the following criteria for flow in a round tube are adopted:

- $\mathrm{Re} < 2100$ – laminar flow,
- $2100 < \mathrm{Re} < 3000$ – transitional flow,
- $\mathrm{Re} > 3000$ – turbulent flow.

Flow coefficient depends on the Reynolds number. If $3 \times 103 < \mathrm{Re} < 10^6$ flow coefficient is defined by the Blasius formula:

$$\lambda = \frac{0.3164}{\sqrt[4]{\mathrm{Re}}}. \tag{7}$$

By calculating the flow coefficient for inner and outer channels, and then substituting all calculated values into Eq. (4), we can get pressure drop of

Table 1: Calculated values of Reynolds numbers.

	Cross-section area [m^2]	Fluid density [kg/m^3]	Fluid velocity [m/s]	Hydraulic diameter [m]	Kinematic viscosity [m^2/s]	Reynolds number
inner channel HP (heating)	2.11×10^{-4}	415.56	0.32	0.0164	0.078×10^{-6}	66532
outer channel LP (heated) model I	1.11×10^{-4}	118.65	2.12	0.0068	0.11×10^{-6}	130914
outer channels LP (heated) model II	4.65×10^{-6}	118.65	3.15	0.0021	0.11×10^{-6}	59918
outer channels LP (heated) model III	4.65×10^{-6}	118.65	3.15	0.0021	0.11×10^{-6}	59918

CO_2 in the channels due to the linear resistance (Tab. 2). For the model III, an additional local pressure loss due to the geometry of outer channels was assumed. The local pressure drop of 33 kPa was estimated based on the Polish Norm'PN-76/M-3404 Pipelines. Principles of pressure drop calculations'.

Table 2: Calculated values of pressure drop.

	Flow coefficient	Pressure drop [Pa]
inner channel HP(heating)	0.020	25
outer channel LP (heated) model I	0.017	21
outer channels LP(heated) model II	0.020	26
outer channels LP(heated) model III	0.020	33026

The boundary condition at the outlet was defined as a pressure outlet with a pressure value of P_{outHP} =11 999 975 Pa for inner channel HP in all three models. Due to the slight pressure drop in the model I outlet pressure is equal to P_{outLPI} = 4 499 979 Pa for outer channel LP, while for model II is equal to P_{outLPI} = 4 499 9974 kPa. The pressure outlet boundary condition for the outflow from outer channels LP in the II model was 4 466 974 Pa.

As a boundary condition at the inlet to the inner channel and outer channels, the following values were used (Tab. 3). Presented boundary

conditions in model II and model III for outer channel were defined in all 16 outer channels.

To calculate the CO_2 flow in the heat exchanger pipes, turbulent flow modeling was applied by using the k-ε turbulent model [19].

Table 3: Boundary conditions for inner and outer channels.

	Mass flow rate [kg/h]	Inlet static pressure [MPa]	Outlet pressure at the outlet [Pa]	Inlet temperature [°C]
inner channel HP (heating)	100.00	12.00	11 999 975	60.00
outer channel LP (heated) model I	100.00	4.50	4 499 979	13.00
outer channel LP (heated) model II	6.25	4.50	44 999 974	13.00
outer channel LP (heated) model III	6.25	4.50	4 466 974	13.00

Standard k-ε model is a semi-empirical model based on equations of transport of turbulence kinetic energy (k) and its dissipation (ε)

$$\frac{\partial}{\partial t}(\rho k)+\frac{\partial}{\partial x_i}(\partial k u_i)=\frac{\partial}{\partial x_j}\left[\left(\mu+\frac{\mu_t}{\sigma_k}\right)\frac{\partial k}{\partial x_j}\right]+G_k+G_b-\rho\varepsilon-Y_M+S_k\,, \quad (8)$$

$$\frac{\partial}{\partial t}(\rho\varepsilon)+\frac{\partial}{\partial x_i}(\partial\varepsilon u_i)= \frac{\partial}{\partial x_j}\left[\left(\mu+\frac{\mu_t}{\sigma_\varepsilon}\right)\frac{\partial\varepsilon}{\partial x_j}\right]+C_{1\varepsilon}\frac{\varepsilon}{k}(G_k+C_{3\varepsilon}G_b)-C_{2\varepsilon}\rho\frac{\varepsilon^2}{k}+S_\varepsilon\,, \quad (9)$$

where: G_k – the generation of turbulence kinetic energy due to the averaged gradient of velocity, G_b – the generation of turbulence kinetic energy due to the buoyancy force, Y_M – source term being the ratio of the turbulence fluctuation dilatation in compressible flow to the overall dissipation coefficient, $C_{1\varepsilon}, C_{2\varepsilon}, C_{3\varepsilon}$ – model constants, $\sigma_k, \sigma_\varepsilon$– the Prandtl numbers for k and ε, respectively, S_k and S_ε – additional user-defined source terms.

The commercial software package was used to solve [18] the energy equation in fluid, in the following form:

$$\frac{\partial}{\partial t}(\rho E) + \nabla \cdot \left(\vec{v}\,(\rho E + p)\right) = \nabla \cdot \left[k_{eff}\nabla T - \sum h_j \underset{J}{\vec{J}} + \left(r_{eff} \cdot \vec{v}\right)\right] + S_h\,, \tag{10}$$

where: k_{eff}– effective conductivity, $\vec{J}$ – diffusion flux, $\vec{v}$ – flow velocity, ρ – density, E – total energy, h – entalphy, S_h – volumetric heat source.

Heat transport in solid was described by the equation:

$$\frac{\partial}{\partial t}(\rho E) + \nabla \cdot \left(\vec{v}\,(\rho h)\right) = \nabla \cdot (k\nabla T) + S_h\,, \tag{11}$$

where k is the thermal conductivity and h is the entalphy, S_h – volumetric heat source.

2.3 Calculation results

The obtained results of temperature distribution calculations in models I, II and III of the IHX counter-current heat exchanger have been presented on the temperature diagram for the inner channel HP (heating) and outer channel LP (heated) and in the form of contours. Tabular form shows the initial flow parameters at the inlet for the inner channel HP, outer channel LP, and calculated parameters at the outlet of the both channels.

The presented temperature distributions for the length of the exchanger $y = 0$ m, corresponding to the inner channel HP inlet outer channels LP, shows a slight difference in temperature at the outflow of outer channels LP between the models I, II and the model II (Fig. 7). Along with the flow of the medium through the inner channel, from $y = 0.0$ m to $y = 1.0$ m, the influence of the low temperature of the material surrounding the inner channel is visible, which reduces the temperature of the medium inside the inner channel HP. At the outlet of the inner channel ($y = 1.0$ m), the influence of changing the geometry in the form of replacing the 1 outer channel 16 outer channels (model II) is noticeable, which results in the lowest temperature of the medium at the outlet of the inner channel HP. In all three models, the flow in inner channels indicates a lower temperature near the wall of the channels. During the flow of fluid in the closed conduit, velocity profiles and the temperature profile are formed in subsequent cross-sections. The maximum velocity and temperature values are located in the

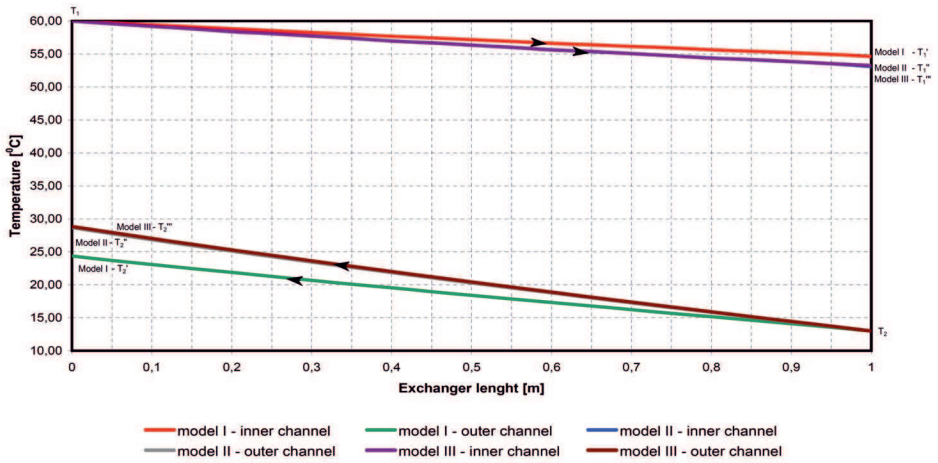

Figure 7: Temperature distribution in inner channels HP (heating) and outer channels LP (heated).

central flow zone, which is the potential core in which the smallest heat exchange occurs. Temperature contours show a larger potential core in the inner channel HP for model I.

For all three models, the largest changes in values of temperature occur in the initial cross sections of inner channels HP (heating) and outer channels LP (heated). This is due to the occurrence of the highest temperature gradient in these places. This phenomenon is particularly well visible in Fig. 8, which contains maps of temperature distribution on the walls of internal HP cables and the selected external conductor LP.

The observed changes in the area of the potential flow of refrigerant stream in the inner channel HP indicate an increase in the refrigeration effect in case of refrigerant flow in model II and model III. These differences are visible in Tabs. 4, 5, and 6. For the same boundary conditions, the difference in temperature at the outlet of the inner channel HP between model I and model II is 1.53 °C, and between model II and model III is 0.14 °C. In the case of an outer channels LP, due to a change in geometry, there was an increase in temperature at the outlet from 24.37 °C (model I) and 28.66 °C (model II) to temperature 28.83 °C (model III).

Using the following formula as

$$\eta_I = \frac{T_1 - T_1'}{T_1 - T_2}100\%\,,\ \eta_{II} = \frac{T_1 - T_1''}{T_1 - T_2}100\%\,,\ \eta_{III} = \frac{T_1 - T_1'''}{T_1 - T_2}100\% \qquad (12)$$

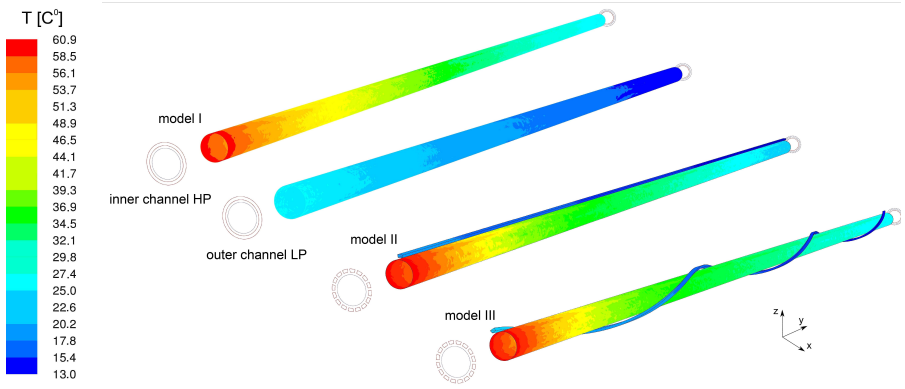

Figure 8: Temperature contours on the walls in inner channels HP (heating) and outer channels LP (heated).

Table 4: Fluid flow parameters in channels of model I.

	Inner channel HP (heating)	Outer channel LP (heated)
$y = 0$ m	inlet	outlet
	$V = 0.32$ m/s	$V = 2.21$ m/s
	$T_1 = 60.00\,^\circ$C	$T_2' = 24.37\,^\circ$C
$y = 1$ m	outlet	inlet
	$V = 0.28$ m/s	$V = 1.94$ m/s
	$T_1' = 54.62\,^\circ$C	$T_2 = 13.00\,^\circ$C

the heat exchanger efficiency for model I, II, and III was calculated:

$$\eta_I = 8.70\%\,, \quad \eta_{II} = 11.21\%\,, \quad \eta_{III} = 11.19\%\,.$$

The heat transfer rate may be obtained from the overall energy balance for the hot fluid. Using the mass flow rate $Q_m = 0.0028$ kg/s, and the specific heat $c_p = 3192$ J/kg K total heat transfer rate was calculated from the formulas:

$$\begin{aligned} q_I &= Q_m c_p \left(T_1 - T_1''\right)\,, \\ q_{II} &= Q_m c_p \left(T_1 - T_1''\right)\,, \\ q_{III} &= Q_m c_p \left(T_1 - T_1'''\right)\,. \end{aligned} \tag{13}$$

Table 5: Fluid flow parameters in channels of model II.

	Inner channel HP (heating)	Outer channel LP (heated)
$y = 0$ m	inlet	outlet
	$V = 0.32$ m/s	$V = 3.43$ m/s
	$T_1 = 60.00\,^\circ$C	$T_2' = 28.66\,^\circ$C
$y = 1$ m	outlet	inlet
	$V = 0.28$ m/s	$V = 2.88$ m/s
	$T_1' = 53.09\,^\circ$C	$T_2 = 13.00\,^\circ$C

Table 6: Fluid flow parameters in channels of model III.

	Inner channel HP (heating)	Outer channel LP (heated)
$y = 0$ m	inlet	outlet
	$V = 0.69$ m/s	$V = 3.47$ m/s
	$T_1 = 60.00\,^\circ$C	$T_2' = 28.83\,^\circ$C
$y = 1$ m	outlet	inlet
	$V = 0.67$ m/s	$V = 2.91$ m/s
	$T_1' = 53.23\,^\circ$C	$T_2 = 13.00\,^\circ$C

from were:

$$q_I = 480.84 \text{ W}, \quad q_{II} = 617.59 \text{ W}, \quad q_{III} = 605.08 \text{ W}.$$

Calculated efficiency and total heat transfer rate show, that the changes in geometry of the heat exchanger outer channels, increases the efficiency of heat exchange by 2.51%. For working conditions presented above, these changes case an increase of total heat transfer rate from 480.84 W for model I to 605.08 W and 617.59 W for model III and model I. These changes take place in the exchanger with a length of 1 m.

3 Conclusion

Paper presents the simulation results of the impact of internal heat exchanger geometry changes on the cooling efficiency of the R744 refrigerant. Geometric models were an accurate reflection of real models and the parameters used to define the boundary conditions were consistent with the design assumptions. The flow calculations were carried out for a transcritical refrigeration cycle, in which the working fluid was CO_2.

The mathematical and numerical model of the internal heat exchanger has been formulated, which enables the multivariant analysis of the flow of R744 refrigerant along with the heat exchange. Based on numerical calculations, it was found that the refrigerant flowing through the counter current internal heat exchanger should be treated as a compressible fluid. In addition, the design and estimated values of the boundary conditions for the flow of R744 refrigerant in the exchanger indicate the flow of supercritical refrigerant in the inner channel HP.

The obtained results of numerical calculations allow to notice the changes in the area of the potential core of the flowing refrigerant stream in the inner channel HP being a heated channel. These changes indicate an increase in cooling capacity in case of refrigerant flow in model II and model III. As a result of changing the geometry in the form of replacing the model outer channel with 16 outer channels obtained was lower temperature at the outlet from the inner channel HP (heating) by 1.53 °C in comparison with the geometry of the 'pipe in pipe' exchanger (model I). Considering the geometry in the form of twisting the outer channels LP (heated), and thus their elongation (model III), does not give significant changes of gas temperature in the inner channel HP (heating) compared with model II.

The change in geometry also increased the heat transfer efficiency by 2.51%, and total heat transfer rate by 136.75 W, which can translate into the efficiency of the car air-conditioning system. The values of pressure differences and temperatures determined from the numerical analysis coincide with the design assumptions.

Presented results in the article suggest that numerical modeling is useful in the aspect of internal heat exchanger optimization.

Acknowledgement Presented article was created as part of the PBS project no /B5/43/2015.

Received 19 January, 2018

References

[1] Furberg R., Palm B., Li S., Toprak M., Muhammed M.: *The use of a nano- and microporous surface layer to enhance boiling in a plate heat exchanger*. J. Heat Trans. **131**(2009). DOI: 10.1115/1.3180702.

[2] Wajs J., Mikielewicz D.: *Effect of surface roughness on thermal-hydraulic characteristics of plate heat exchanger*. Key Engineering Materials **597**(2014), 63–74. DOI: 10.4028/www.scientific.net/KEM.597.63.

[3] Wajs J., Mikielewicz D.:*Influence of metallic porous microlayer on pressure drop and heat transfer of stainless steel plate heat exchanger*. Appl. Therm. Eng. **93**(2016), 1337–1346. DOI: 10.1016/j.applthermaleng.2015.08.101.

[4] Zhang F.Z., Jiang P.X., Lin Y.S., Zhang Y.W.: *Efficiencies of subcritical and transcritical CO_2 inverse cycles with and without an internal heat exchanger*. Appl. Therm. Eng. **31**(2011), 432–438. DOI:10.1016/j.applthermaleng.2010.09.018.

[5] Pettersent J., Hafner A., Skaugen G.: *Development of compact heat exchangers for CO_2 air-conditioning systems*. Int. J. Refrig. **21**(1998), 180–193. DOI: 10.1016/S0140-7007(98)00013-9.

[6] Liu H., Chen J., Chen Z.: *Experimental investigation of a CO_2 automotive air conditioner*. Int. J. Refrig. **28**(2005), 1293–1301. DOI: 10.1016/j.ijrefrig.2005.08.011.

[7] Tamura T., Yakumaru Y., Nishiwaki F.: *Experimental study on automotive cooling and heating air conditioning system using CO_2 as a refrigerant*. Int. J. Refrig. **28**(2005), 1302–1307. DOI: 10.1016/j.ijrefrig.2005.09.010.

[8] Li M.J., Zhang H., Zhang J., Mu Y.T., Tian E., Dan D., Zhang X.D., Tao W.Q.: *Experimental and numerical study and comparison of performance for wavy fin and a plain fin with radiantly arranged winglets around each channel in fin-and channel heat exchangers*. Appl. Thermal Eng. (2018). DOI: 10.1016/j.applthermaleng.2018.01.012.

[9] Tao Y.B., He Y.L., Tao W.Q., Wu Z.G.: *Experimental study on the performance of CO_2residential air-conditioning system with an internal heat exchanger*. Energ. Convers. Manage. **51**(2010) 64–70. DOI: 10.1016/j.enconman.2009.08.024.

[10] Llopis R., Sanz-Kock C., Cabello R., Saanchez D., Torrella E.: *Experimental evaluation of an internal heat exchanger in a CO_2 subcritical refrigeration cycle with gas-cooler*. Appl. Thermal Eng. **80**(2015), 31–41. DOI: 10.1016/j.applthermaleng.2015.01.040.

[11] Sanchez D., Patino J., Llopis R., Cabello R., Torrella E., Fuentes F.V.: *New positions for an internal heat exchanger in a CO_2 supercritical refrigeration plant. Experimental analysis and energetic evaluation.* Appl. Thermal Eng. **63**(2014), 129–139. DOI: 10.1016/j.applthermaleng.2013.10.061.

[12] http://www.chlodnice.net.pl/klimatyzacjasamochodowa.htm (accessed dd.nn.yy).

[13] Wajs J., Mikielewicz D., Fornalik-Wajs E., Bajor M.: *Recuperator with microjet technology as a proposal for heat recovery from low-temperature sources*. Arch. Thermodyn. **36**(2015), 4, 48–63. DOI: 10.1515/aoter-2015-0032.

[14] Mikielewicz D., Wajs J.: *Possibilities of heat transfer augmentation in heat exchangers with minichannels for marine applications*. Pol. Marit. Res. **24**(2017), Spec. iss. 1, 133–140. DOI: 10.1515/pomr-2017-0031.

[15] Rahman M.M., Kariya K., Miyara A.: *An experimental study and development of new correlation for condition heat transfer coefficient of refrigerant inside a multiport minichannel with and without fins*. Int. J. Heat Mass Tran. **116**(2018), 50–60. DOI: 10.1016/j.ijheatmasstransfer.2017.09.010.

[16] Mahmood M., Bhutta A., Hayat N., Bashir M.H., Khan A.R., Ahmad K.N., Khan S.: *CFD applications in various heat exchangers design: A review*. Appl. Thermal Eng. **32**(2012), 1–12. DOI: 10.1016/j.applthermaleng.2011.09.001.

[17] Ituna-Yudonago J.F., Belman-Flores J.M., Elizalde-Blancas F., García-Valladares O.: *Numerical investigation of CO_2 behavior in the internal heat exchanger under variable boundary conditions of the transcritical refrigeration system*. Appl. Thermal Eng. **115**(2017), 1063–1078. DOI: 10.1016/j.applthermaleng.2017.01.042.

[18] Li J., Jia J., Huang L., Wang S.: *Experimental and numerical study of an integrated fin and micro-channel gas cooler for a CO_2 automative air-conditioning*. Appl. Thermal Eng. **116**(2017), 636–647. DOI: 10.1016/j.applthermaleng.2016.12.140.

[19] Ansys Inc (2016): *Ansys Fluent Users Guide*